Journal of Power Sources 185 (2008) 1094–1100

Contents lists available at ScienceDirect

Journal of Power Sources

journal homepage: www.elsevier.com/locate/jpowsour

Simulation of nanostructured electrodes for polymer electrolyte membrane fuel cells

Sanjeev M. Rao, Yangchuan Xing*

Department of Chemical and Biological Engineering, Missouri University of Science and Technology, Rolla, MO 65409, United States

ARTICLE INFO

Article history:
Received 21 July 2008
Accepted 21 July 2008
Available online 31 July 2008

Keywords:
Nanostructured electrodes
Carbon nanotubes
Fuel cells
Catalyst layer
Platinum loading
Simulation

ABSTRACT

Aligned carbon nanotubes (CNTs) with Pt uniformly deposited on them are being considered in fabricating the catalyst layer of polymer electrolyte membrane (PEM) fuel cell electrodes. When coated with a proton conducting polymer (e.g., Nafion) on the Pt/CNTs, each Pt/CNT acts as a nanoelectrode and a collection of such nanoelectrodes constitutes the proposed nanostructured electrodes. Computer modeling was performed for the cathode side, in which both multicomponent and Knudsen diffusion were taken into account. The effect of the nanoelectrode lengths was also studied with catalyst layer thicknesses of 2, 4, 6, and 10 μm. It was observed that shorter lengths produce better electrode performance due to lower diffusion barriers and better catalyst utilization. The effect of spacing between the nanoelectrodes was studied. Simulation results showed the need to have sufficiently large gas pores, i.e., large spacing, for good oxygen transport. However, this is at the cost of obtaining large electrode currents due to reduction of the number of nanoelectrodes per unit geometrical area of the nanostructured electrode. An optimization of the nanostructured electrodes was obtained when the spacing was at about 400 nm that produced the best limiting current density.

1. Introduction

Polymer electrolyte membrane (PEM) fuel cells are being considered as a viable option for power generation and storage. As the fossil fuel crisis becomes more critical, it has become imperative to develop techniques to optimize alternative sources of power generation, so that they would become a cost-effective option for the 21st century. For PEM fuel cells, the cost of the platinum (Pt) catalyst has always hindered their commercialization. PEM fuel cells with Pt loading of 4 mg cm^{-2} was used till recently; even nowadays Pt loading of 0.4 mg cm^{-2} is common and efforts towards further reducing this loading are underway [1].

One way to improve electrode performance is to increase the utilization of the Pt catalyst. There have been suggestions to develop ordered electrode structures, e.g., nanothreads of carbon black (CB) [2] or ordered whiskers [3]. An approximately 20% increase in cell voltage was reported when nanothreads made of CB was employed for electrode fabrication [2]. While CB has been the conventional catalyst support, methods for synthesizing Pt nanoparticles on carbon nanotubes (CNTs) have been successfully demonstrated [4–6]. Most recently, it has been shown that CNTs are much more resistant to electrochemical oxidation than CB in PEM fuel cells [6], making CNTs one of the candidates for catalyst support. Aligned CNTs have been explored for the fabrication of PEM fuel cell catalyst layers with straight pores [7–11]. The inherent advantages of straight pore catalyst layers as compared to the tortuous CB catalyst layers are that they would enhance the transport of oxygen and improve the triple phase boundaries, postulated to result in better catalyst utilization, reduced precious metal loading, and thus higher fuel cell performance.

This work studies a prototype of nanostructured electrodes made from aligned CNTs with Pt uniformly deposited on them. When coated with a proton conducting polymer film (e.g., Nafion) on the Pt/CNTs, each Pt/CNT–Nafion composite acts as a nanoelectrode and a collection of such nanoelectrodes constitutes the proposed nanostructured electrodes. Du et al. [12,13] and Hisaka and Daiguji [14] have recently modeled "orderly structured electrodes" that have straight pores. In their studies, however, Knudsen diffusion was not considered even though the electrode structures they used have pores with sizes comparable to molecular mean free path. Those studies only considered single oxygen component transport without taking into account of the multicomponent gas diffusion for oxygen supply from air. Furthermore, those studies only considered radial diffusion of oxygen through the Nafion film and did not consider the axial gradient of the oxygen concentrations induced by the gas pore diffusion.

* Corresponding author. Tel.: +1 573 341 6772; fax: +1 573 341 4377.
E-mail address: xingy@mst.edu (Y. Xing).

0378-7753/$ – see front matter © 2008 Elsevier B.V. All rights reserved.
doi:10.1016/j.jpowsour.2008.07.062

Nomenclature

c	concentration ($mol\,m^{-3}$)
D	diffusivity ($m^2\,s^{-1}$)
E^0	open circuit potential (V)
F	Faraday's constant ($96{,}487\,C\,mol^{-1}$)
i	current density ($A\,m^{-2}$)
i_0	exchange current density ($A\,m^{-2}$)
K	Henry's constant ($Pa\,m^3\,mol^{-1}$)
L	length along z-axis (m)
M	molecular weight ($kg\,mol^{-1}$)
N	flux ($mol\,m^{-2}\,s^{-1}$)
P	pressure (Pa)
r	radial distance (m)
R	universal gas constant ($8.314\,J\,mol^{-1}\,K^{-1}$)
T	temperature (K)
x	mole fraction
z	axial distance (m)

Greek letters

α	electron transfer coefficient
ε	porosity
η	overpotential (V)
Φ	potential (V)

Subscripts

0	initial value
C	critical
g	gas phase
i, j	index
K	Knudsen diffusion
mem	membrane
N_2	nitrogen
O_2	oxygen
p	pore
ref	reference
solid	solid phase
T	total
w	water vapor

Superscripts

eff	effective
sat	saturation value

In this paper we show that all of the above considerations must be taken into account in modeling the nanostructured electrodes since they have significant effect on the physicochemical properties of the nanostructured electrodes. Meanwhile, we show that optimization of the electrodes is needed in order to exploit the advantages of such nanostructured electrodes to achieve the best performance of PEM fuel cells.

2. Mathematical models and simulation

2.1. Structures of the catalyst layer

The proposed nanostructured electrode based on aligned CNTs is schematically shown in Fig. 1(a). Oxygen in air enters the straight pores between the nanoelectrodes and diffuses to the bottom PEM side (Fig. 1(b)) limited by multicomponent gas phase and Knudsen diffusion [15] in the pores. At each axial location, oxygen will diffuse through the Nafion film to the reaction sites of Pt on the surface of the CNT.

Although it may not be necessary that the CNTs be arranged in any particular fashion, for simulation purposes, only a square grid arrangement of the nanoelectrodes is considered in the present work, i.e., the nanoelectrodes occupy each and every corners of a pattern of square meshes (see Fig. 2(a)). The porosity of such nanostructured electrodes can be easily calculated because the porosity of the catalyst layer depends only on the total number of nanoelectrodes per unit geometrical area of the electrode. The porosity (ε) based on the square grid arrangement is therefore:

$$\varepsilon = 1 - \frac{\text{total area occupied by nanoelectrodes}}{\text{total geometrical area of entire electrode}} \quad (1)$$

The square grid arrangement allows using symmetry in the simulation. By considering only one half of the nanoelectrode and coupling it with the gas pores, a reduced geometry for modeling was obtained (see Fig. 2(b)).

2.2. Basic assumptions

Steady-state and ideal gas behavior were assumed. The Pt catalyst was assumed to be uniformly distributed over the entire CNT surface, allowing application of reaction boundary conditions at every point on the surface. Water transport was neglected under steady state. Ionic resistances were not considered by assuming that the Nafion film is fully saturated with water. Furthermore, an isothermal process was assumed.

2.3. Gas phase transport

Gas transport is via a gas diffusion layer (GDL; carbon paper or cloth) and the straight pores formed between the nanoelectrodes. For steady state, the gas diffusion in the GDL was not considered and a constant composition of the gas mixture was assumed at the interface of the GDL and the nanoelectrodes. Air was the inlet gas mixture at the cathode side and was saturated with water vapor. In the gas pores, multicomponent diffusion of oxygen, water vapor and nitrogen was modeled using the Stefan–Maxwell equations [16–19]. Knudsen diffusion was taken into account in building a generic equation for the gas phase transport [15–17]:

$$\nabla x_i = -\frac{N_i}{c_T D_{K,i}} + \sum_{j \neq 1} \frac{x_i N_j - x_j N_i}{c_T D_{ij}^{eff}} \quad (2)$$

2.4. Nafion phase transport

In the membrane, only oxygen transport was considered. Diffusion was modeled using a simple Fickian diffusion equation. The solution of the Stefan–Maxwell equation gives the distribution of mass fractions of oxygen along the length of each nanoelectrode. They were then converted to mole fractions. The dissolved O_2 concentration at the interface of the Nafion film and the gas pore was defined by the Henry's law [18,19]:

$$c_{O_2} = (1 - x_{N_2} - x_w^{sat}) \frac{P_{O_2}}{K_{O_2}} \quad (3)$$

2.5. Boundary conditions

Referring to Fig. 2, the boundary conditions for solving the set of transport equations are as follows. For the gas phase: at $r = r_A$, a symmetry condition is assumed, giving the no-flux condition at the boundary, i.e.

$$\nabla N_g = 0 \quad (4)$$

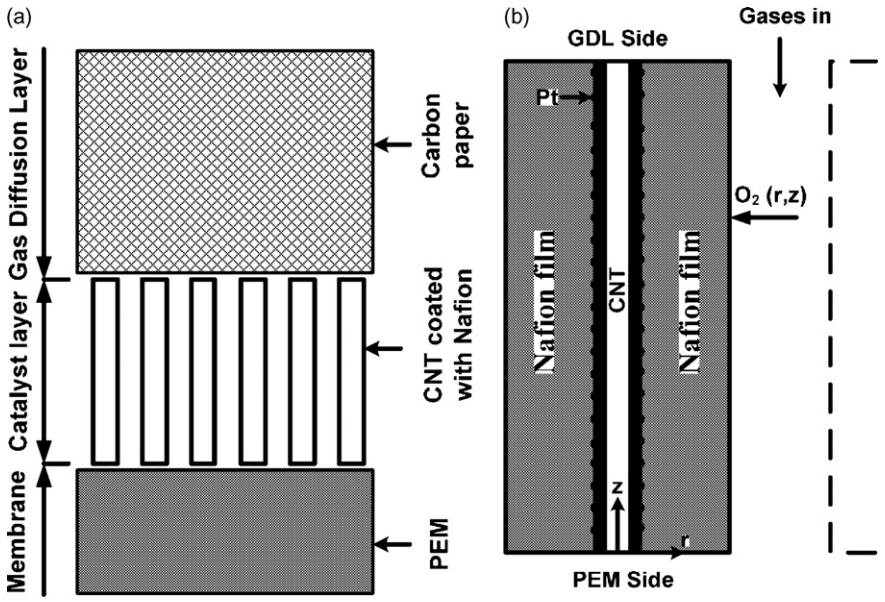

Fig. 1. Proposed nanostructured catalyst layer for PEM fuel cells showing incorporation of aligned CNTs in the catalyst layer (a) and the Nafion film coated CNT as nanoelectrode (b).

At $r = r_B$, the mass fraction of oxygen was solved to give the profile of oxygen mass fraction along the length of the nanoelectrode. This mass fraction was then converted to a mole fraction to calculate the dissolved oxygen concentration at the film–gas pore interface. At $z = 0$, the total gas phase flux is set to zero (Eq. (4)). At $z = L$, the inlet mass fractions were specified for oxygen and water vapor. The mass fraction for nitrogen was calculated by subtracting the sum of the mass fractions of the other two components from unity.

For the Nafion film phase, at $r = r_B$, the dissolved oxygen concentration was calculated by Henry's law using Eq. (3). At $r = r_C$, the flux of dissolved oxygen was calculated from the reaction boundary condition:

$$\nabla N_{O_2} = \frac{i}{4F} \tag{5}$$

This relation comes from Faraday's law [20], i.e., the rate of reaction due to the flow of electrical current is directly proportional to the amount of electricity passed. Using stoichiometry, the reaction rate can be expressed in terms of oxygen consumption. At the two ends where $z = 0$ and $z = L$, the total dissolved oxygen flux is set equal to zero and an insulation boundary condition is used:

$$\nabla \cdot N_{O_2} = 0 \tag{6}$$

2.6. Oxygen reduction reaction (ORR)

The ORR is characterized by a sluggish kinetics and has an exchange current density six orders of magnitude lower than the hydrogen oxidation reaction at the anode [21]. While the polarization curve exhibits two different Tafel slopes, the reaction order with respect to the oxygen partial pressure is one in both potential regions [22]. The rate expression can be written in terms of the Butler–Volmer equation for the cathode kinetics [20]:

$$i = -i_0 \left(\frac{c_{O_2}}{c_{O_2,\text{ref}}} \right) \exp\left(-\frac{\alpha \eta F}{RT} \right) \tag{7}$$

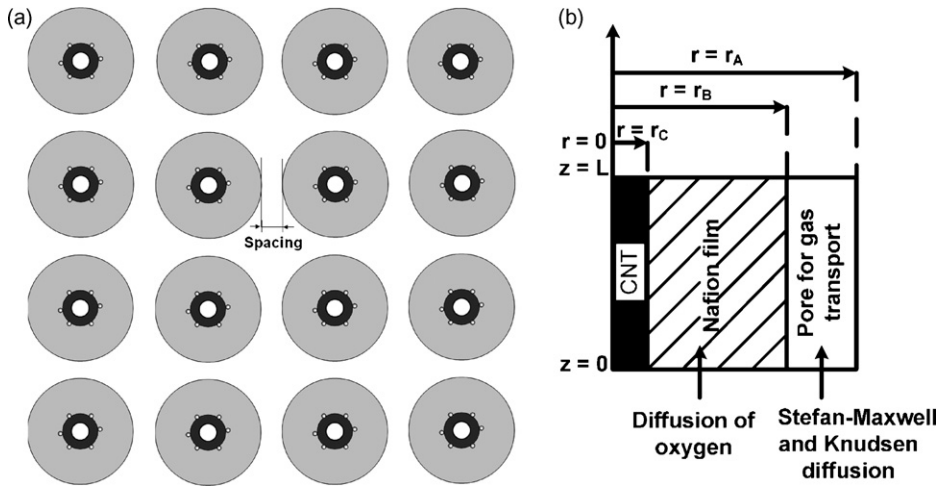

Fig. 2. Square grid arrangement of nanoelectrodes (a) and reduced geometry of a nanoelectrode (b) for modeling and simulation purposes.

2.7. Parameters for simulation

The binary diffusivities for the Stefan–Maxwell equations were calculated using the Slattery–Bird correlation [23]:

$$D_{ij} = \frac{a(T/\sqrt{T_{Ci}T_{Cj}})^b (P_{Ci}P_{Cj})^{1/3}(T_{Ci}T_{Cj})^{5/12}((1/M_i)+(1/M_j))^{1/2}}{P} \quad (8)$$

The diffusion coefficients were corrected for porosity and tortuosity using the Bruggman correlation. However, since in the proposed model the pore network is completely straight along the axial direction and uniformly distributed, the effective diffusion coefficient is

$$D_{ij}^{\text{eff}} = D_{ij}\varepsilon \quad (9)$$

This effective diffusivity was used in the calculation of the symmetric diffusivities.

Knudsen diffusion coefficient varies directly with the mean pore radius (r_p) as [15]:

$$D_{K,i} = \frac{2}{3}\left(\frac{8RT}{\pi M_i}\right)^{1/2} r_p \quad (10)$$

The Knudsen diffusion coefficient was combined with the symmetric diffusivities, giving the effective diffusivity for a component in the gas mixture.

The diffusivity of dissolved O_2 in the Nafion film was estimated from the following equation [18]:

$$D_{O_2} = 3.1 \times 10^{-3} \exp\left(-\frac{2768}{T}\right) \quad (11)$$

Using the oxygen solubility measured at different temperatures by Ogumi et al. [24], the Henry's law constant was calculated from [18]:

$$\ln K_{O_2} = -\frac{666}{T} + 14.1 \quad (12)$$

2.8. Simulation

The proposed model structure was simulated using a commercial CFD package, COMSOL Multiphysics, which utilizes the finite element method to solve differential equations over a given geometry. Since the geometry being simulated was rather simple, default mesh parameters were used with a non-linear solver. The changing parameter was the overpotential defined as

$$\eta = \Phi_{\text{solid}} - \Phi_{\text{mem}} - E^0 \quad (13)$$

where E^0 is the thermodynamic open circuit voltage, and the commonly reported value of 1.23 V was used for the simulation. The parameters used in our simulations are tabulated in Table 1.

Table 1
Parameters used in simulation

Parameter	Value	Units (SI)
Faraday's constant	96,487	C mol^{-1}
Universal gas constant	8.314	J mol^{-1} K^{-1}
Pressure	506,625	Pa
Temperature	353	K
Inlet mass fraction of O_2	0.1447	
Inlet mass fraction of H_2O	0.3789	
Diffusivity of O_2 through H_2O	Eq. (8)	m^2 s^{-1}
Diffusivity of O_2 through N_2	Eq. (8)	m^2 s^{-1}
Diffusivity of H_2O through N_2	Eq. (8)	m^2 s
ORR exchange current density	10^{-5}	A m^{-2}
Diffusivity of O_2 through Nafion	Eq. (11)	m^2 s^{-1}
Henry's constant for O_2	Eq. (12)	Pa m^3 mol^{-1}
Reference O_2 concentration	2.637	mol m^{-3}
Knudsen diffusivity for O_2	Eq. (10)	m^2 s^{-1}
Knudsen diffusivity for H_2O	Eq. (10)	m^2 s^{-1}
Knudsen diffusivity for N_2	Eq. (10)	m^2 s^{-1}

3. Results and discussion

3.1. Effect of spacing between the nanoelectrodes

To investigate the effect of oxygen mass transport on the performance of the proposed nanostructured electrodes, simulations were carried out for different spacing between the nanoelectrodes. To isolate mass transport effects, the kinetic term in Eq. (7) was kept constant by assuming that the overpotential is constant along the length of the CNT nanoelectrode. Mass transport of oxygen to a reaction site on the Pt/CNT surface involves diffusion in the gas pores and subsequent dissolution and diffusion through the Nafion film. In our simulation, the Nafion film thickness is assumed uniform and constant (1 μm) on each of the nanoelectrodes.

Fig. 3 shows the currents plotted on a per CNT (i.e., per nanoelectrode) basis for different spacing at 25, 50, 100, and 400 nm. The current represents the total current obtained by integrating over the entire cylindrical surface of a CNT nanoelectrode. As expected, larger gas pores (i.e., larger spacing) in the catalyst layer allowed better mass transport of the oxygen gas and hence led to better performance of the electrode. However, oxygen mass transport was heavily restricted in the case of smaller spacing due to Knudsen diffusion that was primarily responsible for the poor performance obtained at high overpotentials. This finding is supported by Fig. 4(a), which shows the variation of dissolved oxygen concentrations at the Nafion film–gas interface along the length of the nanoelectrode. The oxygen concentration varied only within 10% for the largest spacing at 400 nm, indicative of the least restriction of mass transfer in this case. However, the oxygen concentration dropped significantly when the spacing was decreased to 100 nm. Further drop was seen for the other two smaller spacing. For air molecules at 80 °C and 5 atm, their mean free path is at about 16 nm. Therefore, a pore size of 25–100 nm would be in the transition regime and Knudsen diffusion limitation plays the most important role. Indeed, very low oxygen concentrations (~0 for the 25 nm spacing) were observed at the bottom of the nanoelectrodes at the film–gas interface. The low oxygen concentrations, coupled with the slow diffusion of dissolved oxygen through the Nafion film, resulted in very low oxygen concentrations at the reaction sites, leading to underutilization of the Pt catalyst present at the bottom portion of the nanoelectrodes.

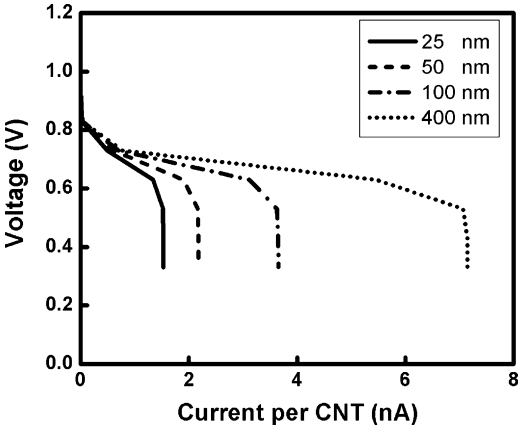

Fig. 3. Polarization characteristics for different CNT spacing. The nanoelectrode length was kept constant at 10 μm. Current plotted on a per CNT basis rather than on a per unit area basis.

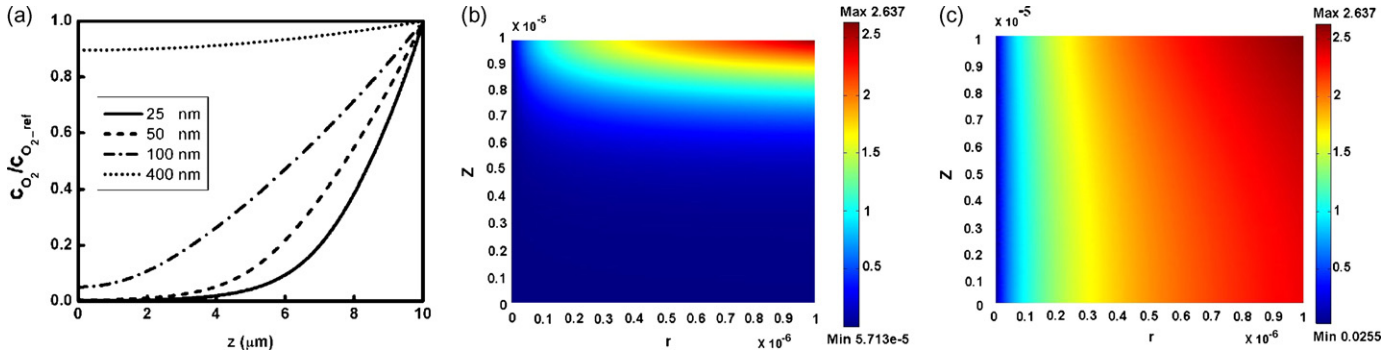

Fig. 4. (a) Effect of pore size (nanoelectrode spacing) on oxygen transport. Oxygen concentration profile plotted at the Nafion film–gas interface along the length of the nanoelectrode. Nanoelectrode length was kept constant at 10 μm and the overpotential was set at 0.7 V. (b and c) Color maps of two-dimensional oxygen concentrations within the Nafion film for a 10 μm long CNT and 25 nm spacing and 400 nm spacing, respectively.

Fig. 4(b) and (c) shows two-dimensional color maps of dissolved oxygen in the Nafion phase for two CNT spacing values of 25 and 400 nm, respectively. As described above, the oxygen concentrations through the Nafion phase are determined by the concentration at the interface and the rate of diffusion through the Nafion film. For the larger spacing, the oxygen concentration was almost constant along the length of the Nafion film–gas interface, and the concentration profile of dissolved oxygen was affected by the low diffusivity only in the radial direction. On the other hand, for the smaller spacing, there was a large gradient in the axial direction of the oxygen concentration at the interface, directly affecting the radial diffusion through the Nafion phase and giving rise a starved oxygen profile as seen in Fig. 4(b). It was noted that the diffusion of oxygen through the Nafion may be much lower than that in the gas phase, especially when the Nafion film thickness is greater than 1 μm [18].

3.2. Effect of Knudsen diffusion

To further understand the role of Knudsen diffusion, simulations were performed with or without Knudsen diffusion being considered in the simulation. This was done for a 10 μm long CNT and 50 nm spacing. Fig. 5 compares the oxygen concentration profiles at the Nafion film–gas interface for the two cases. The oxygen concentration at the bottom in the case with Knudsen diffusion was approximately 10 times lower than the oxygen concentration obtained for the case without Knudsen diffusion. This finding demonstrates the necessity to include Knudsen diffusion in the modeling of the nanostructured electrodes, which was not considered in similar modeling work previously reported [12–14]. Especially, for very small CNT spacing that is comparable to the mean free path of the gas molecules Knudsen diffusion must be included since it becomes substantial. From Eq. (2), it can be deduced that the effect predominant will also be the dominant term in the solution of the overall equation. So if Knudsen diffusion becomes very important, automatically, its dominance would be seen when Eq. (2) is solved for, and vice-versa. Therefore, it is necessary to incorporate both multicomponent and Knudsen diffusion in the mathematical modeling equations.

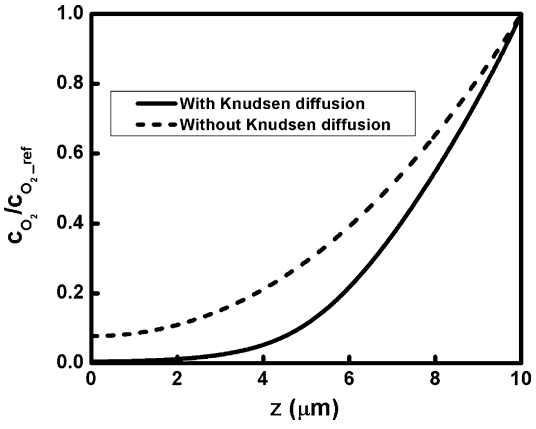

Fig. 5. Effect of Knudsen diffusion for a 10 μm long CNT and 50 nm spacing.

3.3. Effect of different CNT lengths

Thinner catalyst layers should provide better electrocatalytic activity due to reduction of gas transport barriers [25]. One method of addressing the issue of effective catalyst utilization by better oxygen transport and obtaining usable current densities at the same time is by reducing the catalyst layer thickness. This translates into using shorter CNTs to reduce the barrier imposed by oxygen transport in the gas pores. It is postulated that this would also allow for reduced Pt loading and simultaneously improve the utilization of Pt dispersed on the CNT surface. Simulations with different catalyst layer thicknesses (i.e., nanoelectrode lengths) were performed for a fixed CNT spacing (25 nm). In each case, the Pt loading was kept the same for comparison. The results are presented in Fig. 6, which compares the performance of 2, 4, 6, and 10 μm long nanoelectrodes. It can be seen that the electrode performance varies directly with the thickness of the catalyst layer and it was expected

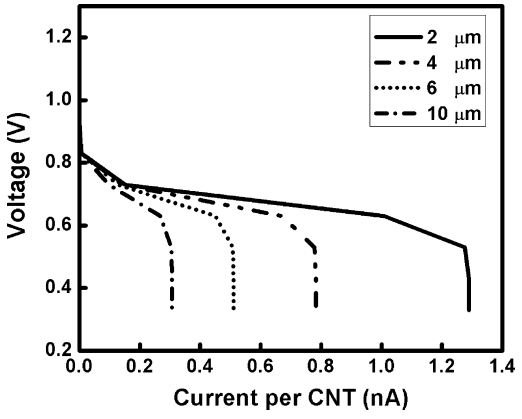

Fig. 6. Effect of catalyst layer thickness on the nanoelectrode performance. The overpotential range is 0.1–0.9 V and spacing is 25 nm, for CNT lengths of 2, 4, 6, and 10 μm.

that the thinner the catalyst layer is, the smaller the diffusion barrier for oxygen transport. This effect should be more pronounced when Knudsen diffusion is dominant, as is the case discussed here in which the spacing is comparable to the mean free path of the gases. At low overpotentials, the assumption of constant kinetics and no ion transport losses led to an overlap of the curves. However, at high overpotentials the 10 μm long CNT was the most severely mass transfer limited when compared to the others. Since the Pt loading was kept the same, the graph also tells that Pt utilization was much better for shorter nanoelectrodes, or thinner catalyst layers.

3.4. Optimization

Oxygen transport in the gas pores is considered to be important to improve fuel cell performance because it affects catalyst utilization. If oxygen cannot reach all the surface reaction sites due to poor mass transfer, it would result in an expensive wastage of the noble metal (Pt) catalyst. From the points discussed above, a logical way in the design of nanostructured catalyst layers would be to keep the nanoelectrode spacing as large as possible for best oxygen transport. However, this will impose a limitation on the number of nanoelectrodes that can be arranged on a certain geometrical area. With large nanoelectrode spacing when the total number of nanoelectrodes per unit geometrical area reduces, the total current density that can be drawn from the entire fuel cell electrode would also be reduced. As a result, optimization should have Pt loading in mind. A higher nanoelectrode density will increase the total Pt loading in the membrane electrode assembly and hence the cost. Therefore, both the Pt loading and the current density need to be compared as functions of spacing (pore size) to determine the spacing that would give a reasonable Pt loading with the best performance for the entire nanostructured electrode.

An example of this optimization approach is illustrated in Fig. 7. For a 10 μm long nanoelectrode with a 1 μm thick Nafion film, the limiting current density and the total Pt loading (both evaluated per unit geometrical electrode surface area) are plotted against the corresponding pore size. While the Pt loading decreases with increasing pore size (spacing) due to the reduction in the CNT number density, the limiting current densities reach a maximum at around 400 nm. This is due to the trade-off between the reduced number of reaction sites (the rates of electrochemical reaction) and the improved mass transport in the pores. It is important to note that a high Pt loading does not necessarily give the best performance when the mass transport is poor, as can be seen from Fig. 7.

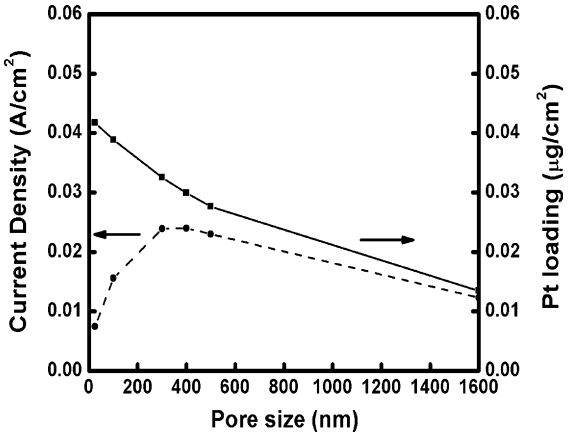

Fig. 7. Limiting current densities and Pt loading per unit electrode area as functions of pore sizes (spacing). The CNT length was kept constant at 10 μm and the Nafion film thickness is maintained at 1 μm for all cases.

3.5. General discussion

While shorter CNTs were observed to result in improved oxygen transport due to a reduced diffusion barrier, the Pt loading that can be obtained on CNTs may pose a limitation. The maximum Pt loading on CNTs (in terms of wt.%) may not satisfy the requirement for the Pt loading in the catalyst layers (in terms of mg cm^{-2}) if the catalyst layer is too thin. According to Xing [4], the Pt loading on multi-wall CNTs that can be achieved without sacrificing the catalyst quality is *ca.* 30 wt.%. For an ideal case, one can calculate the maximum Pt loading on a multi-wall CNT. For example, for 4 nm Pt nanoparticles supported on a 50 nm CNT with an inner diameter of 40 nm, one would get 27 wt.% Pt loading, assuming the nanoparticles are arranged on the CNT surface in a closed cubic pattern when the cylindrical CNT surface is extended flat in two dimensions. For smaller diameter CNTs (i.e., higher specific surface areas), or bigger Pt particles, the Pt loading can be higher.

The aim of this work was to elucidate the effect of mass transport of oxygen in the gas pores on the cathode performance of the nanostructured electrodes. The possible optimization problems that arise from this work need further attention. In addition, the effect of the Nafion film thickness was not studied in this work. Ion transport resistance should be increased in the axial direction by decreasing the Nafion film thickness, but this would also decrease the oxygen diffusion barrier through the film in the radial direction. The interplay of different design parameters will be investigated in a follow-on work that is aimed at a complete optimization of the nanostructured electrodes.

4. Conclusions

In this paper, we have presented a mathematical model that was developed and solved to study the performance of nanostructured electrodes made from aligned CNTs. We have incorporated both multicomponent and Knudsen diffusion in our model formulation. The effect of pore size on oxygen transport in the cathode catalyst layer was studied. The results showed that there is a need to consider Knudsen diffusion when the nanoelectrode spacing is comparable to the mean free path of the gases. It was found that the spacing has a substantial effect on the oxygen transport in the pores, in which a steep gradient of oxygen concentrations was observed at small spacing. This led to an underutilization of the Pt catalyst at the bottom portion of the nanoelectrode. Large spacing improves single nanoelectrode performance, but can decrease the performance of the entire nanostructured electrode since the number of nanoelectrodes per unit geometrical area is reduced. Optimization of the electrode spacing found that a 400 nm spacing produced the best performance in terms of limiting current densities. It was also found that the thickness of the catalyst layer has significant effect on the electrode performance. Shorter thickness led to smaller diffusion barrier. However, the limitation of the Pt catalyst loading on CNTs may restrict on how short the catalyst layer can be.

Acknowledgements

This work is partially supported by a grant from the National Science Foundation (#0522931). We gratefully acknowledge the support of the Intelligent Systems Center at the Missouri University of Science and Technology. We thank professors David B. Henthorn and Frank Liou for helpful discussions.

References

[1] S. Lister, G. Mclean, in: N.P. Brandon, D. Thompsett (Eds.), Fuel Cells Compendium, Elsevier, 2005, pp. 445–446.
[2] E. Middelman, Fuel Cells Bull. 11 (2002) 9.
[3] M.K. Debe, A.K. Schmoeckel, G.D. Vernstrom, R. Atanasoski, J. Power Sources 161 (2006) 1002.
[4] Y. Xing, J. Phys. Chem. B 108 (2004) 19255.
[5] G. Girishkumar, M. Rettker, R. Underhile, D. Binz, K. Vinodgopal, P. McGinn, P. Kamat, Langmuir 21 (2005) 8487.
[6] L. Li, Y. Xing, J. Electrochem. Soc. 153 (2006) 1823.
[7] G. Che, B.B. Lakshmi, E.R. Fisher, C.R. Martin, Nature 393 (1998) 346.
[8] H. Tang, J.H. Chen, Z.P. Huang, D.Z. Wang, Z.F. Ren, L.H. Nie, Y.F. Kuang, S.Z. Yao, Carbon 42 (2004) 191.
[9] C.-L. Sun, L.-C. Chen, M.-C. Su, L.-S. Hong, O. Chyan, C.-Y. Hsu, K.-H. Chen, T.-F. Chang, L. Chang, Chem. Mater. 17 (2005) 3749.
[10] X.R. Ye, L.H. Chen, C. Wang, J.F. Aubuchon, I.C. Chen, A.I. Gapin, J.B. Talbot, S. Jin, J. Phys. Chem. B 110 (2006) 12938.
[11] J. Yang, D.-J. Liu, Carbon 45 (2007) 2843.
[12] C.Y. Du, X.Q. Cheng, T. Yang, G.P. Yin, P.F. Shi, Electrochem. Commun. 7 (2005) 1411.
[13] C.Y. Du, T. Yang, P.F. Shi, G.P. Yin, X.Q. Cheng, Electrochim. Acta 51 (2006) 4934.
[14] M. Chisaka, H. Daiguji, Electrochem. Commun. 8 (2006) 1304.
[15] C.Y. Wang, Chem. Rev. 104 (2004) 4727.
[16] A.Z. Weber, J. Newman, Chem. Rev. 104 (2004) 4679.
[17] A.A. Kulikovsky, J. Divisek, A.A. Kornyshev, J. Electrochem. Soc. 146 (1999) 3981.
[18] D.M. Bernardi, M.W. Verbrugge, J. Electrochem. Soc. 139 (1992) 2477.
[19] D.M. Bernardi, M.W. Verbrugge, AIChE J. 37 (1991) 1151.
[20] A.J. Bard, L.R. Faulkner, Electrochemical Methods: Fundamentals and Applications, 2nd edition, John Wiley, New York, 2001.
[21] S. Mukerjee, S. Srinivasan, in: W. Vielstich, A. Lamm, H.A. Gasteiger (Eds.), Handbook of Fuel Cells—Fundamental Technology and Applications, vol. 2, John Wiley, New York, 2003, pp. 502–519.
[22] M. Gatrell, B. MacDougall, in: W. Vielstich, A. Lamm, H.A. Gasteiger (Eds.), Handbook of Fuel Cells—Fundamental Technology and Applications, vol. 2, John Wiley, New York, 2003, pp. 443–464.
[23] R.B. Bird, W.E. Stewart, E.N. Ligthfoot, Transport Phenomena, John Wiley, New York, 1960.
[24] Z. Ogumi, Z. Takehara, S. Yoshizawa, J. Electrochem. Soc. 131 (1984) 769; S. Mitsushima, N. Araki, N. Kamiya, K. Ota, J. Electrochem. Soc. 149 (2002) 1370.
[25] T.E. Springer, M.S. Wilson, S. Gottesfeld, J. Electrochem. Soc. 140 (1993) 3513.